Spectrum-Flexible Green Light Source Based on SC-PPLN and Superfluorescent Fiber Source

Junhong HE[1], Jun YE[1,2,3], Yanzhao KE[1], Yidong GUO[1], Xiaoya MA[1], Yang ZHANG[1], Junrui LIANG[1], Lei DU[1], Jinhai ZOU[1], Jiangming XU[1*], Jinyong LENG[1,2,3], and Pu ZHOU[1*]

[1]*College of Advanced Interdisciplinary Studies, National University of Defense Technology, Changsha 410073, China*

[2]*Nanhu Laser Laboratory, National University of Defense Technology, Changsha 410073, China*

[3]*Hunan Provincial Key Laboratory of High Energy Laser Technology, National University of Defense Technology, Changsha 410073, China*

[*]Corresponding authors: Jiangming XU and Pu ZHOU   E-mails: jmxu1988@163.com and zhoupu203@163.com

Abstract: The green light source with tailorable temporal coherence has been widely applied in sensing, optical coherence tomography, speckle-free imaging, and partial coherent applications. In this paper, based on a tunable superfluorescent fiber source, we extend the ability of spectral regulation and temporal coherent tunability to the green light band through the second harmonic generation in a step-chirped periodically poled lithium niobate (SC-PPLN) crystal. The wavelength can be tuned from 517.2 nm to 540.0 nm, and the temporal coherence can be controlled by adjusting the bandwidth from 0.23 nm to 13.00 nm. Moreover, we further investigate the output performance at different temperatures and indicate that the appropriate operation wavelength and bandwidth contribute to better power stability under temperature variation. Our work may provide a flexible tunable source for optical coherence tomography, fluorescent imaging, spectroscopy, and so on.

Keywords: Frequency conversion; green light; temporal coherence; PPLN; superfluorescent fiber source

Citation: Junhong HE, Jun YE, Yanzhao KE, Yidong GUO, Xiaoya MA, Yang ZHANG, *et al*. "Spectrum-Flexible Green Light Source Based on SC-PPLN and Superfluorescent Fiber Source," *Photonic Sensors*, 2026, 16(2): 9560004.

1. Introduction

The light source with flexible spectral tunability has a wide range of applications in photoacoustic spectroscopy [1], hyperspectral imaging [2], encrypted communication [3], and laser pumping [4–7]. It is of great importance to extend spectral tunability into the visible region, such as sensing [8], medical imaging [9], and multispectral lidar [10]. A mature and efficient technique to generate visible light is the nonlinear frequency conversion of a near-infrared laser. Notably, broadband, continuous wave (CW) light sources generated in waveguide structures, such as the superluminescent diode (SLD) and superfluorescent fiber source (SFS), have the great potential for realizing spectral regulation because of their flexible filtering characteristics. In addition, compared with the traditional laser with the resonator structure, the broadband source also has the property of low temporal coherence [11],

Received: 27 June 2025 / Revised: 24 October 2025

DOI: 10.26599/PhoS.2026.9560004
Article type: Research article

which makes it a great advantage in low-coherence applications, such as the digital holography [12], uniform illumination in inertial confinement fusion [13], and underwater chaotic lidar [14]. Especially, the frequency converted low temporal coherence chaotic light source could find the important application in temporal ghost imaging (TGI). For example, in 2019, H. Wu, *et al*. [15] demonstrated an innovative extension of temporal ghost imaging based on frequency doubling of a 2 μm multimode quasi-continuous-wave laser with temporal fluctuations and creatively indicated that temporal correlation information can be conveyed to an arbitrary spectral region. In 2024, they [16] further introduced a technique of frequency down conversion TGI and filled the gap of mid-infrared band. Computational TGI in the 3.2 μm–4.3 μm range was demonstrated by employing a conventional telecom modulator to modulate pre-programmed temporal patterns at near-infrared wavelengths.

The SFS based on the ytterbium-doped fiber has been widely concerned because of its unique temporal and broadband output characteristics [17]. The power scaling, spectral regulation techniques, and applications of the SFS have also been rapidly developed [18–26]. Notably, the SFS is a kind of thermal light with a chaotic and stochastic nature. It is generated through the unpredictable quantum process within the fiber, which leads to the emergence of a series of disordered pulses with random intensity at the sub-picosecond scale [27], further enhancing the nonlinear efficiency [28]. Therefore, the SFS is an excellent candidate for generating visible light with flexible spectral tunability by nonlinear frequency conversion.

In recent years, there has been widespread research on spectrum-tunable visible light sources. For example, in 2015, the wavelength tuning range of 574 nm–647 nm was demonstrated from a periodically poled KTP (PPKTP) waveguide by K. A. Fedorova, *et al*. [29]. In 2016, they [30] further presented a tunable dual-wavelength output with a tuning range of 502.1 nm–544.2 nm. In 2018, an orange laser with a tuning range of 593 nm–599 nm from the sum frequency generation (SFG) in a step-chirped PPLN (SC-PPLN) crystal was presented by D. K. Choge *et al*. [31]. In 2019, L. Ebner *et al*. [32] presented a wavelength tunable range of 560 nm–700 nm from a fan-out PPLN crystal with an average power of 1.5 mW. In 2022, H. X. Chen *et al*. [33] demonstrated a broadband yellow-orange light generation with a bandwidth of 5.6 nm and a flatness of less than 1.5 dB. In 2023, H. Wu *et al*. [34] demonstrated a wavelength tuning range of 560 nm–630 nm from a PPLN crystal with 10 separate poled grating periods based on a tunable random Raman fiber laser. In 2024, X. X. Liu *et al*. [35] presented a broadband (from 500 nm to 650 nm) visible random laser through the hybrid SFG and second harmonic generation (SHG) process. In the same year, Y. D. Tao *et al*. [36] proposed a spatially chirped quasi-phase matching (QPM) scheme that enabled ultra-broadband SHG by using a fan-out grating and theoretically demonstrated the limit of the conversion bandwidth of 150 nm. In summary, recent research primarily focused on wavelength tenability, while some focused on broadband generation.

As another dimension of spectral regulation, bandwidth-tunable visible light sources have not been reported. The flexible bandwidth tunability plays a significant role in enhancing light source performance. On the one hand, during power scaling of the SFS, the interaction of the group velocity dispersion and nonlinear effects, such as self-phase modulation and four-wave mixing, results in an optimal pump bandwidth, which ensures the most stable temporal properties [27]. Besides, the spectral power density varies with the bandwidth at the fixed power, further affecting the threshold of stimulated Raman scattering [37]. In addition, the different pumping bandwidths in the random fiber laser affect the shape of the output Raman gain peak, and there is also an optimal bandwidth to achieve the highest spectral purity [38]. Bandwidth-tunable SFSs also have significant applications in photonic computing [39, 40] and ultra-long-distance sensing [41]. For example, by adjusting the feedback bandwidth of the laser source, the sensitivity of the dynamic sensing system increases more than 2.6 times. On the other hand, due to the inverse relationship between the temporal coherence and bandwidth, the tunability of the bandwidth is widely beneficial in partially coherent applications, such as the generation of quantum entangled photon pairs [42], imaging [43–45], and spectroscopy [46, 47]. However, constrained by the strict QPM condition in single-period PPLN, in the case of the SHG of the SFS, increasing the pump bandwidth only extends the spectral coverage. It has little effect on output bandwidth expansion [48]. The substitution of the single-period PPLN with the SC-PPLN affords the light source enhanced spectral and temporal coherent controllability, thereby expanding its potential range of applications.

In this paper, based on a tunable CW SFS, we demonstrate the green light generation with the tunable wavelength and bandwidth using an SC-PPLN crystal to relax the QPM condition. In addition, we investigate the influence of temperature on the output characteristics of the source and indicate that the appropriate operation wavelength and bandwidth contribute to better power stability under dramatic temperature variation. Our work extends the spectral tunability of visible light sources from wavelength tunability to wavelength and bandwidth-independent tunability, as well as providing a flexible visible light source with high power robustness and tailorable temporal coherence, which can satisfy the requirement for temporal coherence in different fields as mentioned above.

2. Experimental setup

Figure 1 shows the schematic of the spectrum-tunable green light source. A linearly polarized bandwidth- and wavelength-tunable SFS with a polarization extinction ratio (PER) of 18.9 dB serves as the seed. A fiber amplifier boosts the seed from a few milliwatts to a maximum of ~6 W. The PER declines to a maximum of 14.0 dB after amplification. To generate tunable green light, the frequency conversion is carried out using an SC-PPLN crystal in a single-pass configuration. The dimensions of the crystal are 20 mm×2 mm×0.5 mm (length×width×height), and the efficient nonlinear coefficient is 14 pm/V. The operation temperature of the crystal is controlled within 20 ℃–200 ℃ by an oven. The poling period is designed as 6.47 μm–7.27 μm, corresponding to the QPM wavelength of 1 040 nm–1 080 nm at the room temperature (25 ℃). The chirp rate of this crystal is 0.04 μm/mm, with a period number of 2 900 and a duty cycle of 53%. The polarization direction is adjusted by a half-wave plate. Two planoconvex lenses are used to collimate and focus the beam on the crystal. The focus length of the first lens is 60 mm. Limited by the size of the clear aperture of the oven, the focus length of the second lens is designed as 300 mm to avoid the beam being blocked. Meanwhile, the long focus length results in lower energy density and conversion efficiency. To ensure that the fundamental wave (FW) is filtered out as completely as possible, two dichroic mirrors are employed to separate the FW from the second harmonic (SH).

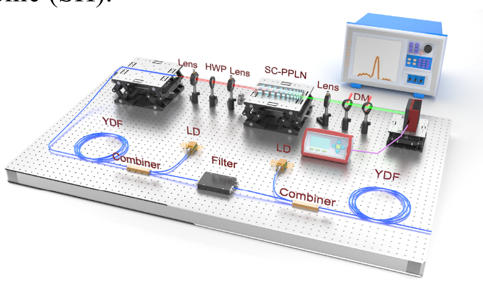

Fig. 1 Experimental setup of the tunable green light source (YDF: ytterbium-doped fiber; LD: laser diode; HWP: half-wave plate; DM: dichroic mirror).

3. Results and discussion

3.1 Wavelength tunability

Firstly, we validate the wavelength tunability of the green light generation. The SFS seed with the bandwidth of 1.0 nm at 3 dB and the wavelength centered at 1 034.4 nm, 1 040 nm, 1 050 nm, 1 060 nm, 1 070 nm, and 1 080 nm are injected into the amplifier. The output spectra are shown in Fig. 2(a), and the percentages represent the in-band power ratio. Notably, the severe amplified spontaneous emission (ASE) occurs when the injected wavelength shifts red, resulting in the in-band power ratio declines from 99.7% to 51.7%. To protect the system, we do not further extend the wavelength tuning range. By inserting a tunable optical filter after the fiber amplifier or optimizing the system parameter such as gain fiber length, the unexpectable ASE can be filtered or reduced.

We stabilize the operating temperature of the crystal at 25 ℃. After the SHG in the crystal, a tunable wavelength from 517.2 nm to 540 nm is demonstrated, as depicted in Fig. 2(b). The SFG occurs between the ASE component and the signal light. For example, when the pump wavelength is 1 080 nm, the spectrum contains ASE with a peak wavelength centered at 1 037 nm, the SFG wavelength of 1 037 nm and 1 080 nm is ~529 nm, corresponding to the output spectrum. When the pump wavelength is 1 070 nm or 1 080 nm, a tiny peak occurs in 515 nm–520 nm, corresponding to the SHG of the peak wavelength of the ASE. The simultaneous occurrence of the SHG and SFG processes indicates the feasibility of realizing multi-wavelength generation in the SC-PPLN crystal.

The power and the conversion efficiency are depicted in Fig. 2(c). As the pumping wavelength is 1 080 nm, due to the low seed power, the pumping power is set to 1.7 W to avoid the damage to the system by the excessive ASE. Due to the deviation from the QPM, efficiency is low at a pumping wavelength of 1 035 nm. The observed decline in conversion efficiency for pump wavelengths beyond 1 060 nm is due to the spatial mismatch between the pump beam waist and the requisite poling period. The pump is focused on the crystal position where the poling period phase-matches 1 060 nm, resulting in the highest power density and thus the peak efficiency. For longer wavelengths, which are phase-matched at positions away from this focus, the pump power density is lower, leading to reduced conversion efficiency. A further increase in output power is limited by pump power.

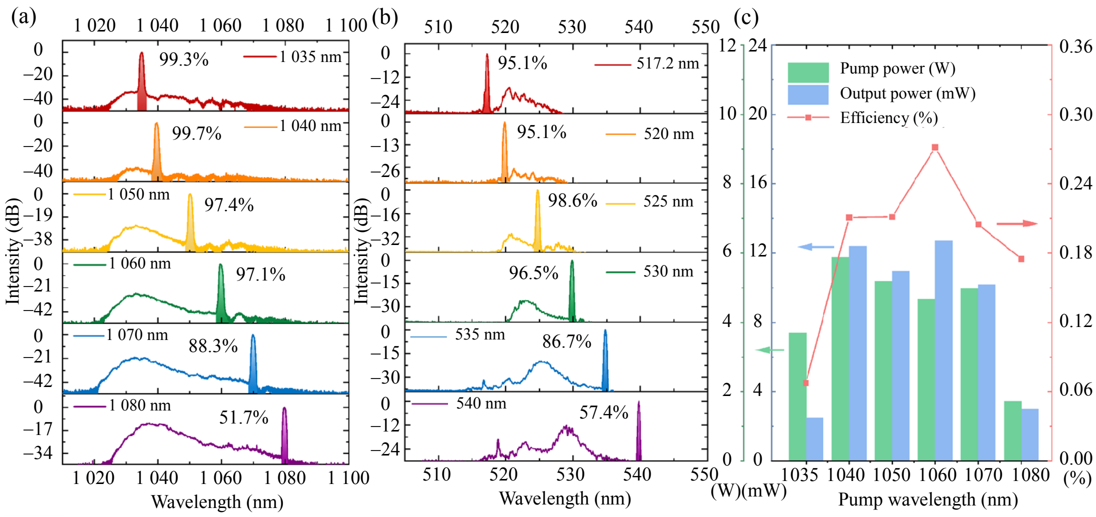

Fig. 2 Wavelength-tunable spectra of (a) the pump light (after the amplifier), (b) the green light (the legends and the percentages respectively represent the wavelength of the signals and the in-band power ratio), and (c) pump power, output power, and efficiency versus different pump wavelengths.

The visible light source has the great potential for power scaling. The FW can be considered as a Gaussian beam, by using a waveguide structure, or optimizing the focal length of the lens, so that the crystal's length is twice the Rayleigh distance [49], and the conversion of the pump light can be significantly improved, leading to a higher conversion efficiency. Specifically, compared to the monolithic crystal, the relationship between the conversion efficiency and the length of the waveguide structure is quadratic rather than linear.

3.2 Bandwidth tunability

The bandwidth tunability of the green light is investigated. By adjusting the bandwidth, it is possible to customize the temporal coherence. According to the Wiener-Khintchine theorem, in the case of a well-behaved stationary random process, the power spectral density is equivalent to the Fourier transform of the autocorrelation function. A broader bandwidth results in a lower power spectral density, which in turn leads to a sharper spike in the autocorrelation curve. In essence, a broader bandwidth denotes a weaker correlation.

The operating temperature of the crystal is controlled at 25 ℃. By adjusting the transmission bandwidth of the tunable filter, the pump wavelength is fixed at 1 055 nm, and the bandwidth can be tuned to 0.7 nm, 1.0 nm, 3.0 nm, 5.5 nm, 10.5 nm, 15.0 nm, 25.0 nm, and 34.1 nm at 10 dB, as shown in Fig. 3(a). The ASE in the 1 025 nm–1 045 nm range appears after power scaling, but the in-band power ratio is still higher than 96.4%. The spectrum of 34.1 nm is the original spectrum of the SFS, since we adjust the available transmission bandwidth of the filter more than 60 nm.

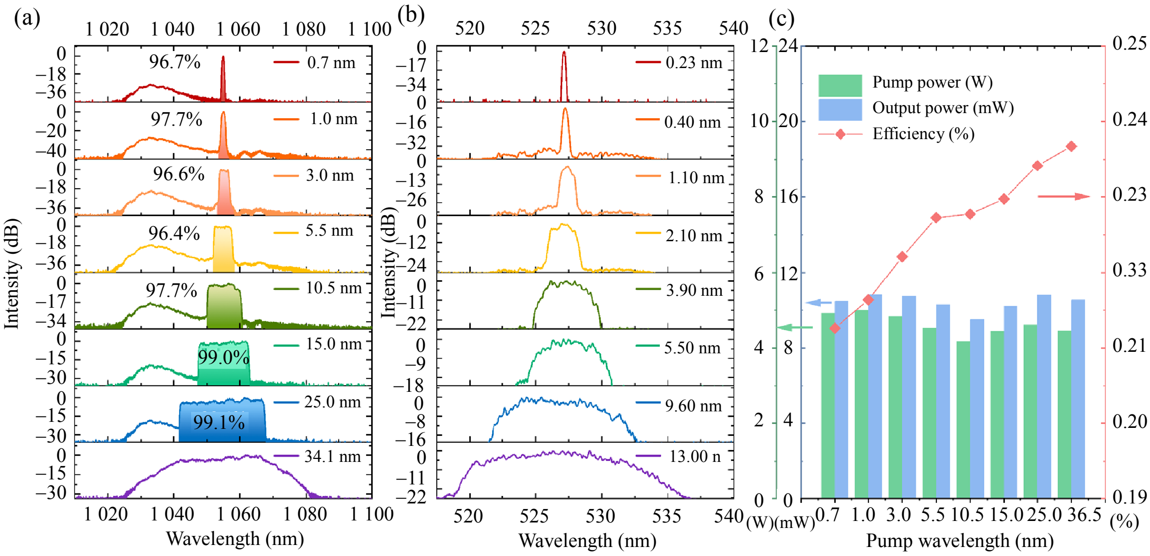

Fig. 3 Linewidth tunable spectra of (a) the pump light (after the amplifier), (b) the green light (the legends and the percentages respectively represent the linewidth of the signals and the in-band power ratio), and (c) pump power, output power, and efficiency versus different pump linewidths.

After frequency conversion, the bandwidth tuning range of 0.23 nm–13.00 nm at 10 dB is demonstrated, as depicted in Fig. 3(b). Notably, compared to approximately rectangular pump spectra, the intensity of the output spectrum's edges is lower than that in the middle, leading to a narrower bandwidth. This is owing to the SFG process dominating the frequency conversion. Essentially, the SFG process is a signal photon merging with a pump photon and annihilating to produce a new sum-frequency photon. The broadband beam contains innumerable photons with different frequencies randomly distributed inside the crystal. Low-frequency photons have a higher probability of annihilating high-frequency photons and generating intermediate-frequency photons, and vice versa. Consequently, the spectral power density of the intermediate wavelength is stronger than that of the edge wavelength, leading to the bandwidth narrowing.

Figure 3(c) exhibits the power of efficiency versus different pump bandwidths. The conversion efficiency increases with the broadening of the bandwidth, which is opposite to the law of the single-period PPLN crystal. Under the narrowband pump, a shorter poling period contributes to the QPM, leading to the short crystal length available to the nonlinear process. Consequently, broadband pump methods in the SC-PPLN crystal can enhance the conversion efficiency by increasing the utilization of a crystal length.

3.3 Power tunability

First, we investigate the power evolution of the green light generation. The bandwidth is adjusted to 1.0 nm and 34.1 nm corresponding to the narrowband and broadband pump methods. To study the inheritance of output stability to the SFS seed, we respectively measure the power fluctuation of the amplified SFS and the output in 2 000 s. The relative standard deviation (RSD, also known as the coefficient of variation, which is defined as the ratio of standard deviation to the mean) of the amplified SFS is 0.20% and 0.44% under broadband and narrowband pumps. Similar to the temporal characteristic of the SFS, the output power exhibits better stability under the broadband pump method, with an RSD of 0.15%, rather than 0.4% under the narrowband pump, as shown in Fig. 4(a). The temporal intensity fluctuation of the SH is influenced by both the pump source and the QPM condition. The broadband pump source delivers a stable temporal intensity to the visible light. Furthermore, the participation of multiple poling periods contributes to the conversion process, resulting in the broadband output being less affected by variations in the QPM condition caused by minor mechanical vibrations or temperature fluctuations. Consequently, employing a broadband pumping method enhances the power stability of the visible output.

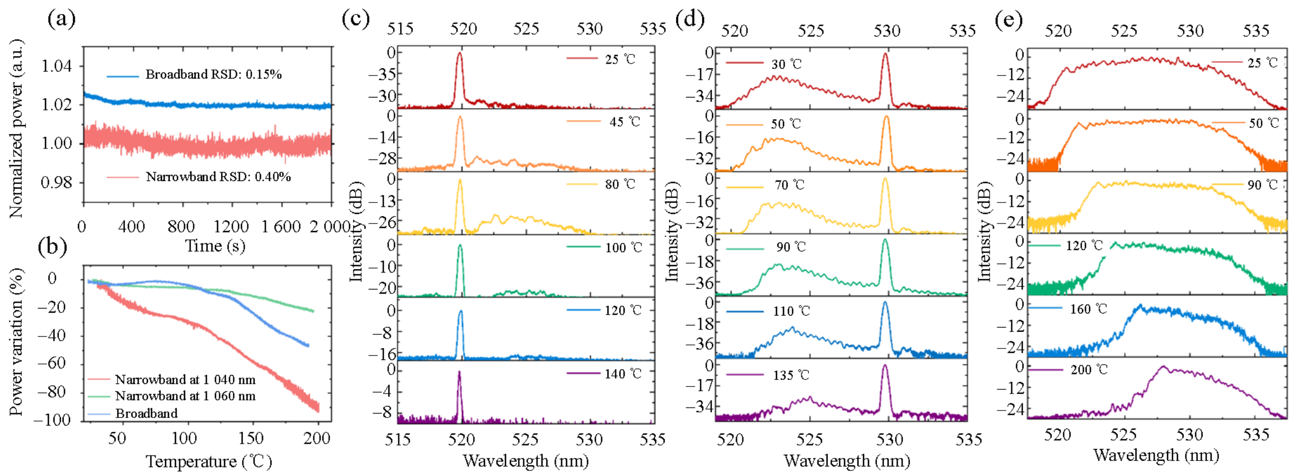

Fig. 4 Power and spectral characteristics of the green light: (a) 2 000 s power stability under broadband and narrowband pump methods, (b) power decline versus temperature under different conditions; spectra at different temperatures operating at (c) 520 nm, (d) 530 nm, and (e) the broadband.

Compared to the single-period PPLN crystal, the SC-PPLN crystal can reduce the stringent requirements for the wavelength and temperature for the QPM. The wavelength of the narrowband seed is determined at 1 040 nm and 1 060 nm, respectively. The power varies with temperature under different conditions as shown in Fig. 4(b). Theoretically, for a certain poling period, the QPM wavelength gets longer with the rising in temperature. Specifically, the poling period of 6.47 μm corresponds to a QPM wavelength of 1 040 nm at 25 ℃ or 1 056 nm at 200 ℃. Therefore, with an increase in the temperature, the spectral power density at 520 nm continuously weakens until it almost disappears at 200 ℃. On the contrary, the output power remains relatively stable, and the power drops to ~80%

under 530 nm operation. The variation trend of the spectrum is consistent with the power, as depicted in Figs. 4(c)–4(e). It can be inferred that the opposite trend occurs when the temperature drops from the room temperature. Under the broadband condition, the power drops to ~50%.

Therefore, selecting the appropriate operating wavelength according to the variation of the ambient temperature helps reduce the sensitivity of power to temperature. Besides, the broadband operation is more suitable for the situation where the temperature dramatically fluctuates around the room temperature. The low sensitivity to the QPM in the SC-PPLN greatly expands the application of visible light sources in temperature-extreme environments.

4. Conclusions

In summary, we demonstrate the green light generation with the wavelength and linewidth tuning ranges of 517.2 nm to 540.0 nm and 0.23 nm to 13.00 nm at 10 dB via the nonlinear process in an SC-PPLN crystal. The temporal coherence of the source can be controlled by adjusting the bandwidth. Moreover, we make a thorough investigation of the spectrum tunability and the output performance versus the temperature. The green light generation inherits the excellent time-domain stability of the SFS and exhibits superb power stability under broadband operation. The power fluctuation remains within 0.15% over 2 000 seconds and within 20% under a temperature variation of 180 ℃. Moreover, we reveal that the appropriate wavelength and bandwidth enhance the power stability under temperature variation. This work provides an effective method for the wavelength- and linewidth-flexible green light generation based on an SFS, which could be advantageous for multiple photonic sensing applications such as ultra-long-distance sensing, where the bandwidth-tunable feature can suppress coherent noise and enhance sensitivity, and interferometric fiber sensing, where the stability of the green light enables high-precision measurement in extreme environments.

Acknowledgment

This work was supported by the National Natural Science Foundation of China (Grant No. 62305391).

Declarations

Conflict of Interest The authors declare that they have no competing interests.

Permissions All the included figures, tables, or text passages that have already been published elsewhere have obtained the permission from the copyright owner(s) for both the print and online format.

Use of AI Statement None.

References

[1] S. Qiao, Y. He, H. Y. Sun, P. Patimisco, A. Sampaolo, V. Spagnolo, *et al.*, "Ultra-highly sensitive dual gases detection based on photoacoustic spectroscopy by exploiting a long-wave, high-power, wide-tunable, single longitudinal-mode solid-state laser," *Light: Science & Applications*, 2024, 13: 100.

[2] J. N. Fang, K. Huang, R. Y. Qin, Y. Liang, E Wu, M. Yan, *et al.*, "Wide-field mid-infrared hyperspectral imaging beyond video rate," *Nature Communications*, 2024, 15: 1811.

[3] M. Z. She, Z. Wang, Y. L. Zhang, A. D. Shi, and W. L. Zhang, "Spectral shaping enabled mode control and information transmission through a multimode optical fiber," *IEEE Photonics Technology Letters*, 2024, 36(5): 357–360.

[4] J. Ye, Y. Zhang, J. R. Lian, X. Y. Ma, J. M. Xu, T. F. Yao, *et al.*, "2 kW random fiber laser based on hybrid Yb-Raman gain," *Chinese Optics Letters*, 2023, 21(9): 090004.

[5] V. Balaswamy, S. Ramachandran, and V. Supradeepa, "High-power, cascaded random Raman fiber laser with near complete conversion over wide wavelength and power tuning," *Optics Express*, 2019, 27(7): 9725–9732.

[6] J. Y. Dong, L. Zhang, H. W. Jiang, X. Z. Yang, W. W. Pan, S. Z. Cui, *et al.*, "High order cascaded Raman

random fiber laser with high spectral purity," *Optics Express*, 2018, 26(5): 5275–5280.

[7] Y. Zhang, J. M. Xu, J. R. Liang, S. C. Li, Jun Ye, X. Y. Ma, *et al*., "High power cladding-pumped low quantum defect Raman fiber amplifier," *Photonics Research*, 2024, 12(5): 995–1003.

[8] K. Monakhova, K. Yanny, N. Aggarwal, and L. Waller, "Spectral DiffuserCam: lensless snapshot hyperspectral imaging with a spectral filter array," *Optica*, 2020, 7: 1298–1307.

[9] T. Zhang, A. M. Kho, and V. J. Srinivasan, "Improving visible light OCT of the human retina with rapid spectral shaping and axial tracking," *Biomedical Optics Express*, 2019, 10(6): 2918–2931.

[10] Y. Chen, Q. Luo, S. Guo, W. Chen, S. Hu, J. Ma, *et al*., "Multispectral LiDAR-based underwater ore classification using a tunable laser source," *Optics Communications*, 2024, 551: 129903.

[11] X. Y. Ma, J. M. Xu, J. Ye, Y. Zhang, Y. Q. Liu, J. Y. Leng, *et al*., "Coherence-tailorable vector fiber source," *Applied Physics Letters*, 2024, 124(9): 091106.

[12] V. Bianco, P. Memmolo, M. Leo, S. Montresor, C. Distante, M. Paturzo, *et al*., "Strategies for reducing speckle noise in digital holography," *Light: Science & Applications*, 2018, 7: 48.

[13] Y. Cui, Y. Q. Gao, D. X. Rao, D. Liu, F. J. Li, L. L. Ji, *et al*., "High-energy low-temporal-coherence instantaneous broadband pulse system," *Optics Letters*, 2019, 44(11): 2859–2862.

[14] L. K. Rumbaugh, E. M. Bollt, W. D. Jemison, and Y. Li, "A 532 nm chaotic lidar transmitter for high resolution underwater ranging and imaging," in *2013 OCEANS – San Diego*, San Diego, USA, 2013, pp. 1–6.

[15] H. Wu, P. Ryczkowski, A. T. Friberg, J. M. Dudley, and G. Genty, "Temporal ghost imaging using wavelength conversion and two-color detection," *Optica*, 2019, 6(7): 902–906.

[16] H. Wu, B. Hu, L. Chen, F. Peng, Z. N. Wang, G. Genty, *et al*., "Mid-infrared computational temporal ghost imaging," *Light: Science & Applications*, 2024, 13: 124.

[17] J. M. Xu, P. Zhou, W. Liu, J. Y. Leng, H. Xiao, and P. F. Ma, "Exploration in performance scaling and new application avenues of superfluorescent fiber source," *IEEE Journal of Selected Topics in Quantum Electronics*, 2018, 24(3): 0900710.

[18] J. Ye, C. C. Fan, J. M. Xu, H. Xiao, J. Y. Leng, and P. Zhou, "2-kW-level superfluorescent fiber source with flexible wavelength and linewidth tunable characteristics," *High Power Laser Science and Engineering*, 2021, 9: e55.

[19] P. Wang, J. K. Sahu, and W. A. Clarkson, "110 W double-ended ytterbium-doped fiber superfluorescent source with M^2=1.6," *Optics Letters*, 2006, 31(21): 3116–3118.

[20] P. Yan, J. Y. Sun, D. Li, X. J. Wang, Y. S. Huang, M. L. Gong *et al*., "933 W Yb-doped fiber ASE amplifier with 504 nm bandwidth," *Optics Express*, 2016, 24(17): 19940–19948.

[21] L. L. Yang, J. D. Wu, N. Li, Q. W. Duan, D. Y. Liu, L. L. Miao, *et al*., "Watt-level superfluorescent fiber source near 3 μm," *Optics Letters*, 2021, 46(11): 2778–2781.

[22] W. Gao, W. H. Fan, Y. P. Zhang, P. Ju, B. Y. Zhao, P Wu, *et al*., "High-power tunable sub-nm narrowband near diffraction-limited superfluorescent fiber source based on a single-lens spectral filter," *Optics Communications*, 2020, 463: 125359.

[23] Y. Zheng, Y. Yang, J. Wang, M. Hu, G. Liu, X. Zhao, *et al*., "10.8 kW spectral beam combination of eight all-fiber superfluorescent sources and their dispersion compensation," *Optics Express*, 2016, 24(11): 12063–12071.

[24] J. X. Song, H. S. Wu, J. Ye, J. M. Xu, H. W. Zhang, and P. Zhou, "High power linearly polarized Raman fiber laser with stable temporal output," *Photonic Sensors*, 2019, 9(1): 43–48.

[25] B. Han, S. Dong, Y. Liu, and Z. N. Wang, "Cascaded random Raman fiber laser with low RIN and wide wavelength tunability," *Photonic Sensors*, 2022, 12: 220414.

[26] J. He, J. Ye, Y. Ke, Y. Guo, X. Ma, Y. Zhang, *et al*., "High power spectrum-tailorable superfluorescent fiber source," *Optics & Laser Technology*, 2024, 178: 111237.

[27] J. Ye, X. Ma, Y. Zhang, J. Xu, H. Zhang, T. Yao, *et al*., "From spectral broadening to recompression: dynamics of incoherent optical waves propagating in the fiber," *PhotoniX*, 2021, 2(1): 15.

[28] N. Valero, D. Marion, J. Lhermite, J. C. Delagnes, W. Renard, R. Royon, *et al*., "High-power amplified spontaneous emission pulses with tunable coherence for efficient non-linear processes," *Scientific Reports*, 2021, 11: 4844.

[29] K. A. Fedorova, G. S. Sokolovskii, P. R. Battle, D. A. Livshits, and E. U. Rafailov, "574–647 nm wavelength tuning by second-harmonic generation from diode-pumped PPKTP waveguides," *Optics Letters*, 2015, 40(5): 835838.

[30] K. A. Fedorova, C. D. Wong, C. M. Kaleva, I. O. Bakshaev, D. A. Livshits, and E. U. Rafailov, "Tunable single- and dual-wavelength SHG from diode-pumped PPKTP waveguides," *Optics Letters*, 2016, 41(21): 5098–5101.

[31] D. K. Choge, H. X. Chen, B. L. Tian, Y. B. Xu, G. W. Li, and W. G. Liang, "Multi-peak tunable CW orange laser based on single-pass sum frequency generation in step-chirped MgO: PPLN," *Optical and Quantum Electronics*, 2018, 50: 226.

[32] L. Ebner and A. Zumbusch, "Yb fiber-based laser source for tunable, narrow bandwidth picosecond

pulses in the visible," *Optics Letters*, 2019, 44(9): 2290–2293.

[33] H. X. Chen, H. Z. Huang, J. X. Cheng, X. B. Zhang, X. K. Feng, X. Cheng, *et al*., "Broadband yellow-orange light generation based on a step-chirped PPMgLN ridge waveguide," *Optics Express*, 2022, 30(18): 32110–32118.

[34] H. Wu, W. Z. Wang, B. Hu, Y. Li, K. Tian, R. Ma, *et al*., "Widely tunable continuous-wave visible and mid-infrared light generation based on a dual-wavelength switchable and tunable random Raman fiber laser," *Photonics Research*, 2023, 11(5): 808–816.

[35] X. X. Liu, W. H. Hao, Z. H. Yang, M. W. Mao, and Y. L. Tang, "Ultra-broadband visible random laser generation via hybrid SHG and SFG processes," *Journal of Lightwave Technology*, 2024, 42(6): 2131–2136.

[36] Y. D. Tao, W. T. Zhu, Y. F. Zhang, J. G. Ma, J. Wang, P. Yuan, *et al*., "Ultrabroadband second-harmonic generation via spatiotemporal-coupled phase matching," *Chinese Optics Letters*, 2024, 22(1): 011901.

[37] W. Liu, P. F. Ma, H. B. Lv, J. M. Xu, P. Zhou, and Z. F. Jiang, "Investigation of stimulated Raman scattering effect in high power fiber amplifiers seeded by narrow-band filtered superfluorescent source," *Optics Express*, 2016, 24(8): 8708–8717.

[38] J. Ye, J. M. Xu, J. X. Song, Y. Zhang, H. W. Zhang, H. Xiao *et al*., "Pump scheme optimization of an incoherently pumped high power random fiber laser," *Photonics Research*, 2019, 7(9): 977–983.

[39] B. W. Dong, F. Brückerhoff-Plückelmann, L. Meyer, J. Dijkstra, I. Bente, D. Wendland, *et al*., "Partial coherence enhances parallelized photonic computing," *Nature,* 2024, 632: 55–62.

[40] F. Brückerhoff-Plückelmann, H. Borras, B. Klein, A. Varri, M. Becker, J. Dijkstra, *et al*., "Probabilistic photonic computing with chaotic light," *Nature Communications*, 2024, 15: 10445.

[41] Y. F. Qi, S. T. Lin, J. J. Zhang, P. Wang, and Z. N. Wang, "Impact of feedback bandwidth on Raman random fiber laser remote-sensing," *Optics Express*, 2022, 30(12): 21268–21275.

[42] S. Arahira and H. Murai, "Wavelength conversion of incoherent light by sum-frequency generation," *Optics Express*, 2014, 22(11): 12944–12961.

[43] D. Paganin and K. A. Nugent, "Noninterferometric phase imaging with partially coherent light," *Physical Review Letters*, 1998, 80(12): 2586–2589.

[44] J. N. Clark, X. Huang, R. Harder, and I. K. Robinson, "High-resolution three-dimensional partially coherent diffraction imaging," *Nature Communications*, 2012, 3: 993.

[45] H. Q. Chen, X. X. Ji, Y. S. Wang, Z. Y. Chen, O. Sasaki, and J. X. Pu, "Investigation on intracavity SHG with controllable coherence in a degenerate laser," *IEEE Journal of Quantum Electronics*, 2020, 56(1): 1–6.

[46] C. Bourassin-Bouchet and M. E. Couprie, "Partially coherent ultrafast spectrography," *Nature Communications*, 2015, 6: 6465.

[47] T. Tashima, Y. Mukai, M. Arahata, N. Oda, M. Hisamitsu, K. Tokuda, *et al*., "Ultra-broadband quantum infrared spectroscopy," *Optica*, 2024, 11(1): 81–87.

[48] J. H. He, J. Ye, Y. Z. Ke, X. Y. Ma, Y. Zhang, J. R. Liang, *et al*., "Influence of wavelength, linewidth, and temperature on second harmonic generation of a superfluorescent fiber source," *Optics Express*, 2024, 32(3): 3266–3277.

[49] G. D. Boyd and D. A. Kleinman, "Parametric interaction of focused Gaussian light beams," *Journal of Applied Physics*, 1968, 39(8): 3597–3639.